Atmos. Chem. Phys. Discuss., 6, 9967–9994, 2006
www.atmos-chem-phys-discuss.net/6/9967/2006/

Atmospheric Chemistry and Physics Discussions

A study of polar ozone depletion based on sequential assimilation of satellite data from the ENVISAT/MIPAS and Odin/SMR instruments

J. D. Rösevall, D. P. Murtagh, J. Urban, and A. K. Jones

Department of Radio & Space Science, Chalmers Univ. of Technology, Göteborg, Sweden

Received: 3 July 2006 – Accepted: 9 October 2006 – Published: 10 October 2006

Correspondence to: J. D. Rösevall (rosevall@rss.chalmers.se)

Abstract

The objective of this study is to demonstrate how polar ozone depletion can be mapped and quantified by assimilating ozone data from satellites into the wind driven transport model DIAMOND, (Dynamical Isentropic Assimilation Model for OdiN Data). With access to a large set of satellite data, ozone fields can be built up that are far less noisy than the individual satellite ozone profiles. The transported fields can subsequently be compared to later sets of incoming satellite data so that the rates and geographical distribution of ozone depletion can be determined. By tracing the amounts of solar irradiation received by different air parcels in a transport model it is furthermore possible to study the photolytic reactions that destroy ozone.

In this study, destruction of ozone that took place in the Antarctic winter of 2003 and in the Arctic winter of 2002/2003 has been examined by assimilating ozone data from the ENVISAT/MIPAS and Odin/SMR satellite-instruments. Large scale depletion of ozone has, as expected, been observed in the Antarctic polar vortex of 2003 when sunlight returned after the polar night. Ozone depletion in the range 10–20% was furthermore observed on the 475 K potential temperature level in the central regions of the 2002/2003 Arctic polar vortex.

1 Introduction

Massive photochemical depletion of ozone has been observed in the Antarctic polar vortex during late winter and spring seasons for more than two decades (Farman et al., 1985). Indications of corresponding, albeit smaller depletion of ozone in the Arctic spring has also been found (Rex et al., 1998; Newman et al., 2002). The standard explanation for these phenomena involves activation of chlorine reservoir species in heterogeneous reactions that take place on aerosol-particle surfaces in so called polar stratospheric clouds. Polar stratospheric clouds consist of both crystalline and liquid aerosols of nitric- and sulphuric-acid that form inside the polar vortex during the polar

ACPD

6, 9967–9994, 2006

winter night. Since it is less stable and therefore warmer, far fewer polar stratospheric clouds however form in the Arctic polar vortex than in its Antarctic counterpart.

Since polar vortex air masses are separated from the surrounding stratosphere, relatively high concentrations of reactive Cl_x species can build up during the dark winter months. When sunlight returns after the winter, the reactive species destroy ozone by acting as catalysts in photochemical reactions. To quantify the depletion of ozone one must somehow follow air parcels that move in the stratosphere so they can be sampled at consecutive times. A Lagrangian approach to this problem has been outlined by Rex et al. (1998). It involves calculating three dimensional trajectories of air parcels that undergo wind driven advection on isentropic surfaces and vertical transport due to radiative cooling of the winter stratosphere. Ozone destruction in the air parcels is subsequently estimated by comparing balloon sonde measurements at the start and at the end of the calculated trajectories. It should be possible to use this technique also with satellite data but individual satellite measurements are by and large more noisy which makes the method more difficult to implement. Ozone depletion is instead often estimated by taking daily averages of all satellite measurements inside the polar vortex. To keep track of the polar vortex which moves, changes its shape and sinks during the winter, stratospheric constituents with low chemical reactivity can be followed (Proffitt et al., 1993). Sampling the entire polar vortex at once does however give a rather low spatial resolution. The method outlined in Rex et al. (1998) suffers on the other hand from low temporal resolution as well as from low spatial coverage since the number of balloon sondes is limited.

The objective of this study is to demonstrate how ozone depletion can be mapped and quantified by assimilating ozone data from satellites into a wind driven transport model. With access to large sets of satellite data, ozone fields can be built up that are far less noisy than the individual satellite ozone profiles. The transported fields can subsequently been compared to later sets of incoming satellite data for the purpose of determining the rates and geographical distribution of polar ozone depletion.

A low-diffusive transport and assimilation model, DIAMOND(Dynamical Isentropic

Assimilation Model for OdiN Data), has been developed to accomplish the strategy outlined above. It has been used to study the destruction of polar ozone in the Antarctic winter of 2003 and in the Arctic winter of 2002/2003 by assimilating ozone profiles from the Odin/SMR and ENVISAT/MIPAS satellite-instruments. Nitrous oxide profiles from Odin/SMR have been assimilated in parallel with the ozone data for the purpose of tracing horizontal as well as vertical movement in the polar vortex.

2 The DIAMOND Model

The DIAMOND model has been designed to accomplish low-dispersive off-line wind-driven ozone transport in the lower stratosphere. Horizontal advection has been modeled on 12 separate isentropic surfaces between 425 and 975 K which correspond roughly to altitudes in the range 15 to 35 km. See Fig. 1. Chemistry has been omitted from the model since polar ozone reactivity tends to be rather low at altitudes below 35 km except when fast photolytic destruction of ozone occurs in ClO_x activated air masses in the early spring.

Vertical transport has been omitted from the model since potential temperatures are conserved in dry air under adiabatic conditions. An exception to near adiabatic conditions occurs however during the polar winter night when there is strong radiative cooling of air masses inside the polar vortex. The diabatic cooling can cause potential temperatures to decrease at rates of 20–40 K per month during early winters. The descent is thus rather slow compared to horizontal transport but it should still be monitored when studying polar ozone depletion that can take place over several months. In this study the vertical transport has been monitored by keeping track of chemically stable N_2O that has been assimilated in parallel with the ozone fields.

2.1 Transport model

The DIAMOND model has been dedicated for studying the polar regions. Horizontal transport has therefore been modeled on a square grid that is centred over one pole and extends to the equator. See Fig. 2. With a grid like this it has been possible to achieve high spatial resolution without using ultra fine time discretisation which is generally a limiting factor for latitude/longitude grids that have very fine zonal grid spacing near the poles. The simplicity of the grid has also facilitated implementing the advection scheme. The fact that the grid does not provide global coverage is on the other hand a disadvantage but it is tolerable since equatorial air masses need several weeks to reach the regions surrounding the polar vortex. Another obvious disadvantage is that the square shape of the grid is distorted in the equatorial region. By transforming the off-line wind fields to the local non-Cartesian coordinate systems one can eliminate transportation errors but the use of a rhomboid grid adds some numerical diffusivity to the transport scheme. The square shape of the grid is however well retained over the polar regions where ozone depletion occurs. A grid spacing of 167×167 km (over the pole) and a time-step of 10 min length has been used in this study.

Horizontal off-line wind driven advection has been implemented using the Prather transport scheme (Prather, 1986). It is a mass conservative Eulerian type of transport scheme that achieves very low numerical diffusivity by storing and transporting the first and second order spatial derivatives of tracer fields as well as the average tracer concentration in each grid-box. The Prather scheme is thus much more time consuming than a simple upstream transport scheme but the low numerical diffusivity achieved is essential when quantifying ozone depletion processes that proceed over several months. Wind fields obtained from the European Centre for Medium-range Weather Forecasts, ECMWF, have been used to force the advection scheme in this study.

ACPD
6, 9967–9994, 2006

2.2 Assimilation scheme

Satellite data are assimilated into the DIAMOND model using a sequential algorithm that can be described as a variant of the familiar Kalman filter. A field containing estimates of the errors in the model is thus built up and transported alongside the ozone field for the purpose of weighting in new data in an optimal way. In each model time-step the assimilation algorithm updates the subset of grid points that are located within 3000 km of any satellite observations that have been made. New data is weighted in according to the formula below where $\boldsymbol{X_b}$ is a column vector containing the subset of model grid-points that are affected by assimilation, $\boldsymbol{X_a}$ is the same subset of the model grid after assimilation and $\boldsymbol{Y}$ is a vector containing the satellite data to be assimilated. $\mathbf{H}$ is an operator for linear interpolation from the model grid to the locations of the satellite measurements and $\mathbf{W}$ is an optimal weighting matrix that is derived in each time-step (Daley, 1991).

$$\boldsymbol{X_a} = \boldsymbol{X_b} + \mathbf{W}(\boldsymbol{Y} - \mathbf{H}(\boldsymbol{X_b})) \tag{1}$$

The optimal weighting matrix, $\mathbf{W}$, is derived using estimates of the noise in the satellite measurements, given in a covariance matrix $\mathbf{R}$, and estimates of the errors in the model field, given by two covariance matrices $\mathbf{S_{bo}}$ and $\mathbf{S_{oo}}$.

$$\mathbf{W} = \mathbf{S_{bo}}(\mathbf{S_{oo}} + \mathbf{R})^{-1} \tag{2}$$

To be more precise, $\mathbf{S_{bo}}$ is a cross covariance matrix of the model errors in the vector $\boldsymbol{X_b}$ and the model errors at the points of satellite observations, $\mathbf{H}$ ($\boldsymbol{X_b}$). $\mathbf{S_{oo}}$ is on the other hand a covariance matrix for the errors in $\mathbf{H}$ ($\boldsymbol{X_b}$) alone.

$$\mathbf{R} = \left\langle (\boldsymbol{Y} - \boldsymbol{Y_t})(\boldsymbol{Y} - \boldsymbol{Y_t})^T \right\rangle \tag{3}$$

$$\mathbf{S_{bo}} = \left\langle (\boldsymbol{X_b} - \boldsymbol{X_t})(\mathbf{H}(\boldsymbol{X_b}) - \mathbf{H}(\boldsymbol{X_t}))^T \right\rangle \tag{4}$$

ACPD
6, 9967–9994, 2006

$$\mathbf{S_{oo}} = \left\langle (\mathbf{H}(\boldsymbol{X_b}) - \mathbf{H}(\boldsymbol{X_t}))(\mathbf{H}(\boldsymbol{X_b}) - \mathbf{H}(\boldsymbol{X_t}))^T \right\rangle \quad (5)$$

$\boldsymbol{X_t}$ and $\boldsymbol{Y_t}$ in the formulae above denote the true atmospheric concentrations of the tracer at the grid-points and at the points of satellite observations respectively and $\langle\ \rangle$ denotes the operator for expectation values.

To derive **W** it is thus necessary to somehow estimate the matrixes $\mathbf{S_{bo}}$ and $\mathbf{S_{oo}}$. A computationally efficient solution to this problem can be implemented by estimating the correlation between different points in the model, (indexed i and j), with an empirical correlation function $F(i, j)$ so that only σ_i, (the estimated error standard deviations in the actual grid points), have to be stored and transported (Menard et al., 2000).

$$\mathbf{S}_{ij} = \sigma_i \sigma_j * F(i, j) \quad (6)$$

The correlation function, $F(i, j)$, must be chosen empirically to fit the particular transport model that it is used with. One way to simplify this process is to assume that $F(i, j)$ is a function of the geographical distance, r_{ij}, between the two grid points i and j. This methodology has for example been described in (Khattatov et al., 2000) where several different function types were evaluated as candidates for $F(r_{ij})$. One function that they found favourable was the Gaussian shaped function. It has therefore been used in the Diamond model. The function is fitted to the transport model by means of tuning the parameter, L.

$$F(i, j) = \exp\left(-\frac{r_{ij}^2}{2L^2}\right) \quad (7)$$

Assimilation of new data is obviously a process that lowers the standard deviation estimates in the σ field. Consequently Kalman filtering theory describes how the field should be updated when assimilation has occurred.

$$\boldsymbol{\sigma_a}^2 = \boldsymbol{\sigma_b}^2 - diag(\mathbf{W}\mathbf{S}_{\mathbf{bo}}^T) \quad (8)$$

ACPD
6, 9967–9994, 2006

EGU

There are on the other hand also factors like chemical processes in the stratosphere and imperfections in the transport scheme that makes it necessary to add a growth term to the σ field. In the DIAMOND model, linear increment with time has been used to approximate the growth of uncertainty in the tracer fields.

$$\sigma_{(t+\Delta t)} = \sigma_t + k_\sigma * \Delta t \tag{9}$$

Both L and k_σ are parameters that must be tuned empirically. Ideally they should be set to values that minimise the difference between model forecasts, $\mathbf{H}_n(X)$, and individual satellite observations, y_n, in a least squares sense.

$$\sum_{n=1}^{N} (y_n - \mathbf{H}_n(X))^2 \Big/ N \tag{10}$$

This least squares value is however not very sensitive to either L or k_σ once the assimilation model has run for a few days. The error growth rate, k_σ, has therefore been tuned to a value for which agreement is achieved between the model error standard deviation estimates, σ_x, and the observed variance between model and satellite observations.

L has on the other hand been derived by evaluating the quadratic form in expression (11). The dimensionless values given by the expression are expected to be distributed according to the so called χ^2-function of order equal to M (the number of elements in $\boldsymbol{Y}$) if the matrices $\mathbf{R}$ and $\mathbf{S_{oo}}$ provide correct estimates of the error covariances for the vectors $\boldsymbol{Y}$ and $\boldsymbol{H(X)}$ respectively. $\mathbf{R}$ is not controlled by any assimilation parameter since it is supplied in the satellite data. The non diagonal elements in $\mathbf{S_{oo}}$ are on the other hand functions of L. The parameter has thus been tuned to a value for which the expected χ^2 -distribution was found, (see Fig. 3).

$$(\boldsymbol{Y} - \mathbf{H}(X))^T (\mathbf{S_{oo}} + \mathbf{R})^{-1} (\boldsymbol{Y} - \mathbf{H}(X)) \sim \chi^2_M \tag{11}$$

ACPD
6, 9967–9994, 2006

3 Odin/SMR

The Odin satellite, launched in 2001 as a joint venture by the national space agencies of Sweden, Canada, Finland and France, completes ∼15 near-terminator polar orbits per day with descending nodes at 06:00 h local solar time. Its payload consists of two different limb scanning instruments, SMR (Sub-Millimetre Radiometer) and OSIRIS (Optical Spectrograph/InfraRed Imaging System), that obtain vertical profiles of ozone and other trace species in the middle atmosphere (Murtagh et al., 2002). The SMR instrument is however also used for radio-astronomy which means that 50% of the satellites operational time is used for astrophysics instead of Earth observations.

The OSIRIS instrument detects visible and infrared light scattered from the sun. It can therefore not make observations when the sun is below the horizon of the satellite in the winter hemisphere. Consequently no data from the OSIRIS instrument has been used in this study.

The SMR instrument comprises four tunable Schottky-diode single-sideband heterodyne microwave receivers. In the basic mode for stratospheric observations, two of the receivers covering the 486–504 and 541–558 GHz frequency bands respectively, are used to detect microwave emission lines in the spectra of O_3, N_2O, ClO and HNO_3. Two separate lines, centred at 501.5 and 544.9 GHz respectively, are observed in the spectrum of ozone. The ozone data used in this study have been retrieved from the 501.5 GHz line using the Chalmers-v2.0 retrieval scheme (Urban et al., 2006; Eriksson et al., 2005). In the polar regions the ozone profiles thus obtained cover altitudes in the range 12–50 km with ∼3 km altitude resolution. The N_2O data used in this study have been retrieved from a line at 502.3 GHz using the same software. The N_2O profiles cover altitudes in the range 12–60 km with ∼1.5 km altitude resolution.

The distribution of Odin/SMR ozone observations minus DIAMOND model forecasts on the 475 K level is presented in Fig. 4. One can clearly see that the Odin/SMR ozone data is much more noisy than the ENVISAT/MIPAS data that is also studied.

ACPD
6, 9967–9994, 2006

4 ENVISAT/MIPAS

The ENVISAT satellite, launched in 2002 by the European Space Agency (ESA), completes ~15 polar orbits per day with descending nodes at 10:00 h local solar time. Its mission comprises monitoring the land, ice, oceans and atmosphere of the Earth providing data for environmental research. Ten different instruments are included in its payload, three of which GOMOS, MIPAS and SCIAMACHY were designed to study trace gases in the atmosphere.

The MIPAS instrument, (Michelson Interferometer for Passive Atmospheric Sounding), is a passive limb scanning high-resolution Fourier transform spectrometer for the middle infrared region (Endemann, 1999). The instrument was primarily designed to retrieve atmospheric profiles of ozone, water vapour nitric acid, methane and nitrous oxide but it can also provide estimates of temperatures and CFC concentrations in the stratosphere. The data retrieval scheme for ozone and other trace gases is described in Ridolfi et al. (2000). The MIPAS ozone profiles used in this report have been produced using the 4.61 version of the retrieval software and cover the altitude range 8–55 km with 3 km altitude resolution. The distribution of MIPAS ozone observations minus DIAMOND model forecasts on the 475 K level is presented in Fig. 4.

5 Ozone depletion in the Antarctic Winter of 2003

The ozone destruction that occurred in the Antarctic polar vortex of 2003 has been studied by comparing assimilated fields of ozone to ozone fields that have been passively transported from 1 August of that year. The time evolution on the 475 K potential temperature level can be seen in Fig. 5. The top fields in the figure represent the hours of sunlight that had fallen on the air masses in the model since 1 August. The middle row contains assimilated fields of ozone profiles from ENVISAT/MIPAS and the bottom row contains fields passively transported from 1 August without any new data assimilated into them. The initial ozone fields were obtained by assimilating ozone profiles

into the DIAMOND model for more than two months prior to 1 August. Substantial depletion of ozone can be seen in the polar vortex as the air masses become exposed to sunlight. Large scale ozone destruction thus occurs first at the outer edges of the vortex in August and reaches the central polar vortex by the end of September.

Quantitative estimates of the 2003 Antarctic ozone depletion have been made using assimilated fields of ozone data from ENVISAT/MIPAS and Odin/SMR. See Figs. 6 and 7 respectively. Significant differences can be seen between the two sets of estimates. Both sets indicate that ozone destruction started at the outer edges of the polar vortex in August and spread to the central vortex by mid September. The Odin/SMR estimates however indicate far less depletion than the ENVISAT/MIPAS estimates on the 425 and 475 K potential temperature levels.

An obvious prerequisite for obtaining correct estimates of polar ozone depletion using the method presented above is that the satellite instruments used to collect the ozone data detects all ozone depletion that occurs in a quantitatively correct manner. Constant systematic errors in the satellite data can be tolerated but they must not change over the time period that is studied.

The model fields obtained from ENVISAT/MIPAS and Odin/SMR data have been compared to balloon sonde measurements in Fig. 8. The stars represent balloon sonde measurements made at the south pole and the solid lines represent the ozone concentrations found in the DIAMOND assimilation model over the same location. One can see that the assimilated fields obtained using ENVISAT/MIPAS data agree fairly well to the balloon sondes. There is some disagreement on the 525 K level from late September throughout October but otherwise the model results seem to be well fitted to the sonde data. The assimilated fields obtained using Odin/SMR data do on the other hand not agree well with the sonde measurements on the 425, 475 and 525 K potential temperature levels. The assimilated ozone concentrations are too low before large scale depletion occurs and too high after the ozone hole has formed. Estimates of ozone depletion made using this set of data will thus underestimate the ozone depletion. These biases are currently under investigation by the Odin/SMR science team at

the Chalmers University of Technology.

6 Vertical transport in the polar vortex

The ozone depletion estimates presented in Figs. 6 and 7 were made without taking vertical transport into account. During the polar night, the potential temperatures in the polar vortex decrease due to radiative cooling. Air masses thus slowly move across the potential temperature levels used in the DIAMOND model possibly causing errors in the estimates of ozone depletion presented above.

To keep track of the vertical transport processes, N_2O data from Odin/SMR have been assimilated in parallel with the ozone fields. The mixing ratio of N_2O decreases rapidly with altitude since the species is destroyed by high energy UV-radiation in the upper stratosphere. N_2O is on the other hand chemically inert at lower altitudes and in the polar night and can therefore be used as a passive tracer to monitor transport in the polar vortex. Time series of model vortex average N_2O mixing ratios are plotted in Fig. 9. The vortex averages are defined as the average mixing ratio on the 30 million km^2 area with lowest N_2O concentration on each potential temperature level in the DIAMOND model. N_2O samples of equal size have thus been obtained on all levels in the vortex which makes the sample averages relevant for tracing vertical transport in it. Using samples with constant size throughout the months studied is furthermore consistent way of defining the polar vortex. The 30 million km^2 samples are however well retained within the vortex borders as defined by the contours of maximum gradient in the N_2O fields.

The N_2O mixing ratios in Fig. 9 decrease rapidly from May to late July, indicating fast radiative cooling of the polar vortex during this period. From early August to late October the mixing ratios were on the other hand more stable which indicates that transport between different potential temperature levels was slow. By following the vortex average N_2O mixing ratios we estimate that the potential temperatures on all four levels described in Fig. 9 decreased with ~10 K during August and remained stable

ACPD
6, 9967–9994, 2006

in September and October. Vertical transport is therefore a small error source in this analysis since the difference in polar vortex ozone mixing ratios between model levels was generally less than 20%.

7 Ozone depletion in the Arctic Winter of 2002/2003

Temperatures in the 2002/2003 Arctic polar vortex were low enough to sustain polar stratospheric clouds from mid November to mid January leading to 15–30% activation of chlorine reservoir species in January and February (EORCU, 2003). ClO_x catalyzed photochemical destruction of ozone was therefore possible in sunlit areas of the vortex.

Assimilated fields of ENVISAT/MIPAS and Odin/SMR data have been compared to ozone sonde measurements made at Ny-Ålesund (79° N, 12° E), see Fig. 10. The ENVISAT/MIPAS fields agree well to the sonde data while discrepancies can be seen between the sondes and the Odin/SMR fields. Neither sonde nor satellite data however show any clear signs of ozone depletion. (Ny-Ålesund was located outside the polar vortex for a 10 day period in the latter half of February causing low ozone mixing ratios on the 425 K potential temperature level and elevated mixing ratios on the levels above during this period.)

Ozone depletion occurring in the Arctic polar vortex after 1 January 2003 have furthermore been studied using the methodology outlined in Sect. 5. The time evolution on the 475 K potential temperature level is presented in Fig. 12. Ozone destruction in the range 10–30%, depending on instrument, can be seen in the central polar vortex by the end of January. There seems on the other hand not to have been any significant destruction of ozone near the outer edges of the vortex which is unlike the pattern observed in the southern hemisphere. One plausible explanation for the difference is that large scale chlorine activation only occurred in the colder central regions of the 2002/2003 Arctic polar vortex.

Decreasing potential temperatures in the polar vortex however introduced non-negligible errors into the passively transported fields that were used to produce the

ozone depletion estimates in Fig. 12. The time evolution of vortex average N_2O mixing ratios in the Arctic winter of 2002/2003 are presented in Fig. 11. Substantial vertical transport across the model potential temperature levels are indicated by the falling mixing ratios. One can estimate that the potential temperatures decreased with around 30 K from 1 January to mid February. The ozone mixing ratios in the 475 K passive field should therefore have increased during the same period due to vertical transport of more ozone rich air masses from higher altitudes. Due to this effect, Fig. 12 underestimates the depletion of ozone with ~5%. The difference between the estimates made using ENVISAT/MIPAS and Odin/SMR data are however larger than the effects introduced by decreasing potential temperatures.

8 Conclusions

In this study we have demonstrated how the DIAMOND transport and assimilation model can be used to map and quantify Antarctic as well as Arctic polar ozone depletion. Systematic errors in the assimilated satellite data have introduced some discrepancies in the analysis but the method nevertheless looks promising. Not implementing vertical transport across isentropic levels in the DIAMOND model have furthermore introduced some smaller biases in the analysis. This will be addressed in the future.

When studying the Antarctic polar vortex of 2003 we, as expected, saw ozone destruction spatially confined to regions where sunlight had returned after the polar night. Large scale ozone depletion thus started at the outer edges of the vortex in August and reached the central region by mid september. We were on the other hand not able to observe any ozone depletion near the vortex outer edges in the Arctic winter of 2002/2003. In the central regions of the vortex we could however estimated 10–20% ozone depletion during the months of January and February using ENVISAT/MIPAS data and 20–30% depletion using Odin/SMR data.

Acknowledgements. Odin is a Swedish-led satellite project funded jointly by the Swedish National Space Board (SNSB), the Canadian Space Agency (CSA), the National Technology

Agency of Finland (Tekes) and the Centre National d'etudes Spatiales (CNES) in France. We thank the European Space Agency (ESA) for providing ENVISAT/MIPAS data. ECMWF wind and temperature fields have been downloaded from the data centre at Norsk Institutt for LUftforskning (NILU) operated under the EU supported SCOUT project. This work has also been supported by the Chalmers Environmental Initiative (www.miljo.chalmers.se/cei).

References

Daley, R.: Atmospheric data analysis, Cambridge University Press, 1991. 9972

Endemann, M.: MIPAS instrument concept and performance, Proceedings of the European Symposium on Atmospheric Measurements from Space, ISSN 1022-6656 (European Space Research and Technology Center–European Space Agency, Noordwijk, The Netherlands, 1999) , WPP-161, Vol. 1, 29–43, 1999. 9976

Eriksson, P., Jiménez, C., and Buehler, S.: Qpack: A tool for instrument simulation and retrieval work, J. Quant. Spectrosc. Radiat. Transfer., 91, 47–61, doi:10.1016/j.jqsrt.2004.05.050, 2005. 9975

EORCU: The Northern Hemisphere Stratosphere in the 2002/2003 winter, Tech. rep., The European Ozone Research Coordinating Unit, Department of Chemistry, University of Cambridge, UK, 2003. 9979

Farman, J. C., Gardiner, B. G., and Shanklin, J. D.: Large losses of total ozone in Antarctica reveal seasonal ClO_x/NO_x interaction, Nature, 315, 207–210, 1985. 9968

Khattatov, B. V., Lamarque, J.-F., Lyjak, L. V., Menard, R., Levelt, P., Tie, X., Brasseur, G. P., and Gille, J. C.: Assimilation of Satellite Observations of Long-lived Chemical Species in Global Chemistry Transport Models, J. Geophys. Res., 105(D23), 29135, doi:10.1029/2000JD900466, 2000. 9973

Menard, R., Cohn, S. E., Chang, L.-P., and Lyster, P. M.: Stratospheric assimilation of Chemical Tracer Observations Using a Kalman Filter, parts i and ii, Mon. Wea. Rev., 128, 2654–2686, 2000. 9973

Murtagh, D., Frisk, U., Merino, F., Ridal, M., Jonsson, A., Stegman, J., Witt, G., Eriksson, P., Jiménez, C., Megie, G., de la Noë, J., Ricaud, P., Baron, P., Pardo, J. R., Hauchcorne, A., Llewellyn, E. J., Degenstein, D. A., Gattinger, R. L., Lloyd, N. D., Evans, W. F. J., McDade, I. C., Haley, C. S., Sioris, C., von Savigny, C., Solheim, B. H., McConnell, J. C., Strong, K.,

Richardson, E. H., Leppelmeier, G. W., Auvinen, H., and Oikarinen, L.: An overview of the Odin atmospheric mission, Can. J. Phys., 80, 309–319, 2002. 9975

Newman, P. A., Harris, N. R. P., Adriani, A., Amanatidis, G. T., Anderson, J. G., Braathen, G. O., Brune, W. H., Carslaw, K. S., Craig, M. S., DeCola, P. L., Guirlet, M., Hipskind, R. S., Kurylo, M. J., Küllmann, H., Larsen, N., Megie, G. J., Pommereau, J.-P., Poole, L. R., Schoeberl, M. R., Stroh, F., Toon, O. B., Trepte, C. R., and Roozendael, M. V.: An overview of the SOLVE/THESEO 2000 campaign, J. Geophys. Res., 107(D20), 8259, doi:10.1029/2001JD001303, 2002. 9968

Prather, M. J.: Numerical Advection by Concervaion of Second-Order Moments, J. Geophys. Res., 91(D6), 6671–6681, 1986. 9971

Proffitt, M. H. K., Aiken, J. J., Margitan, M., Lovenstein, J. R, and Podolske, A.: Ozone loss inside the northern polar vortex during the 1991–1992 winter, Science, 261, 1150–1154, 1993. 9969

Rex, M., von der Gathen, P., Harris, N. R. P., Lucic, D., Knudsen, B. M., Braathen, G. O., Reid, S. J., De Backer, H., Claude, H., Fabian, R., Fast, H., Gil, M., Kyrö, E., Mikkelsen, I. S., Rummukainen, M., Smit, H. G., Stähelin, J., Varotsos, C., and Zaitcev, I.: In situ measurements of stratospheric ozone depletion rates in the Arctic winter 1991/1992: A Lagrangian approach, J. Geophys. Res., 103(D5), 5843, doi:10.1029/97JD03127, 1998. 9968, 9969

Ridolfi, M., Carli, B., Carlotti, M., von Clarmann, T., Dinelli, B. M., Dudhia, A., Flaud, J. M., Morris, P. E., Raspollini, P., Stiller, G., and Wells, R. J.: Optimized forward model and retrieval scheme for MIPAS near-real-time data processing, Appl. Opt., 39, 1323–1340, 2000. 9976

Urban, J., Lautie, N., Le Flochmoen, E., Murtagh, D., Ricaud, P., De La Noe, J., Dupuy, E., Drouin, A., El Amraoui, L., Eriksson, P., Frisk, U., Jimenez, C., Kyrola, E., Llewellyn, E. J., Megie, G., Nordh L., and Olberg, M.: The northern hemisphere stratospheric vortex during the 2002/03 winter: Subsidence, chlorine activation and ozone loss observed by the Odin Sub-Millimetre Radiometer, Geophys. Res. Lett., 31, L07103, doi:10.1029/2003GL019089, 2004.

Urban, J., Murtagh, D., Lautié, N., Barret, B., Dupuy, E., de La Noë, J., Eriksson, P., Frisk, U., Jones, A., le Flochmoën, E., Olberg, M., Piccolo, C., Ricaud, P., and Rösevall, J.: Odin/SMR Limb Observations of Trace Gases in the Polar Lower Stratosphere during 2004–2005, Proc. ESA Atmospheric Science Conference, 8–12 May 2006, Frascati, Italy, European Space Agency publications, ESA-SP-628, http://earth.esrin.esa.it/workshops/atmos2006/participants/68/paper_frascati2006.pdf, 2006. 9975

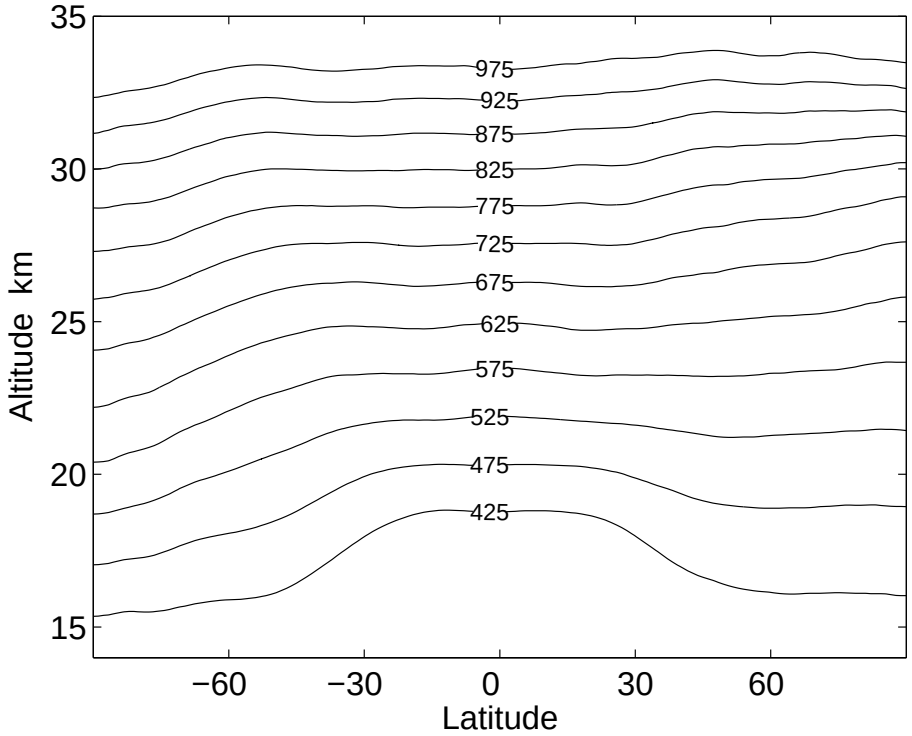

Fig. 1. Average December altitudes of the isentropic levels used in the DIAMOND model. Potential temperatures in Kelvin.

ACPD
6, 9967–9994, 2006

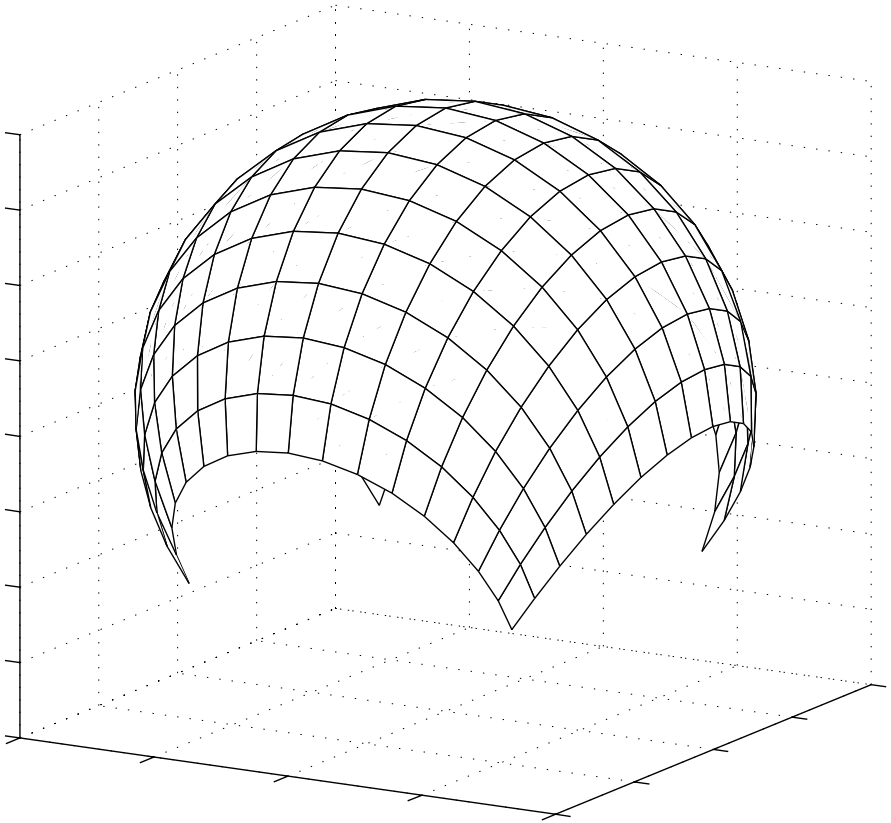

Fig. 2. The shape of the grid used in the DIAMOND model.

ACPD
6, 9967–9994, 2006

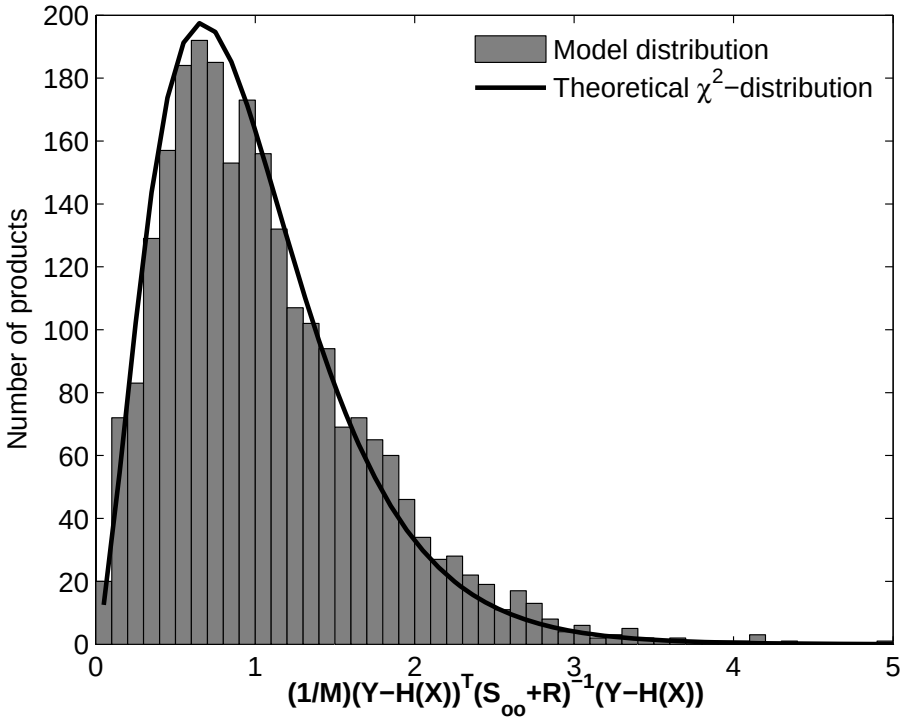

Fig. 3. The correlation distance parameter L has been tuned to a value for which the distribution of the dimensionless quadratic form $(\boldsymbol{Y} - \mathbf{H}(X))^T(\mathbf{S_{oo}} + \mathbf{R})^{-1}(\boldsymbol{Y} - \mathbf{H}(X))$ fits a theoretical χ^2-distribution.

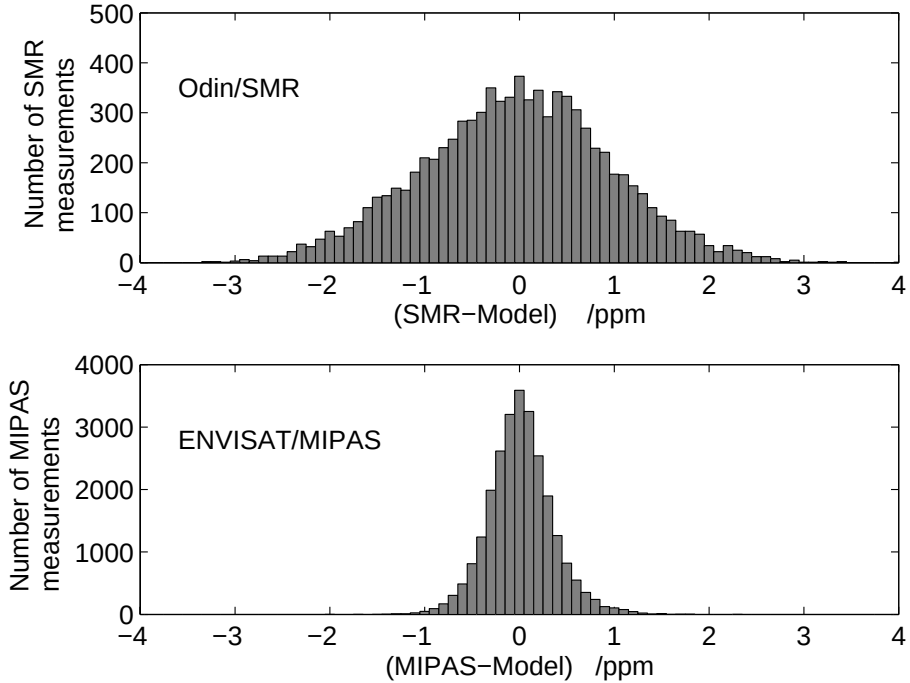

Fig. 4. Observations minus model background on the 475 K potential temperature level. All observations included in the histograms were made north of 30° N during January, February and March of 2003.

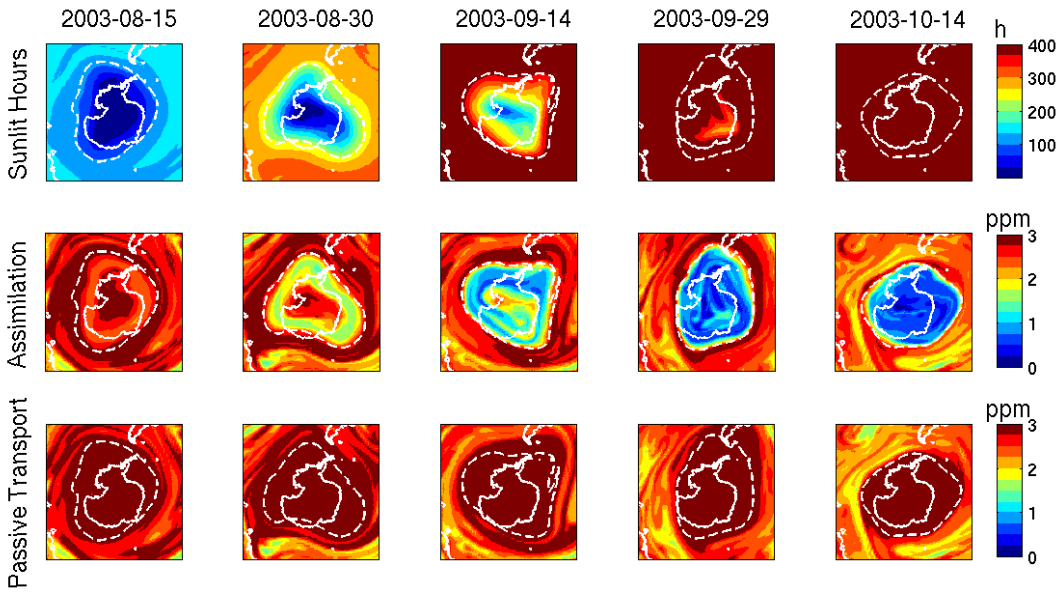

Fig. 5. Assimilated fields of ozone on the 475 K potential temperature level compared to fields passively transported from 1 August of 2003. The fields in the top row represent the number of hours of sunlight that has fallen on the air masses in the model since 1 August, the middle row contains assimilated fields of ozone profiles from ENVISAT/MIPAS and the bottom row contains fields passively transported from 1 August without any new data assimilated into them. The dashed lines outline the border of the polar vortex.

ACPD
6, 9967–9994, 2006

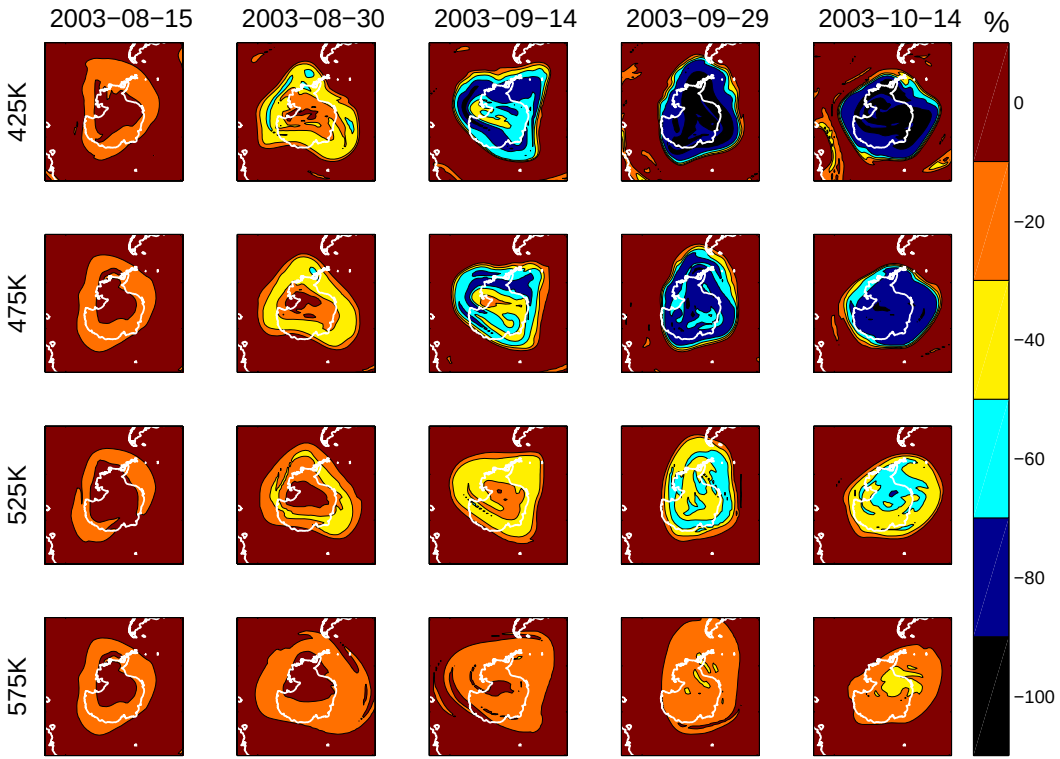

Fig. 6. Estimates of ozone depletion in the 2003 Antarctic spring made by comparing assimilated fields of Odin/SMR data to fields passively transported from 1 August.

ACPD
6, 9967–9994, 2006

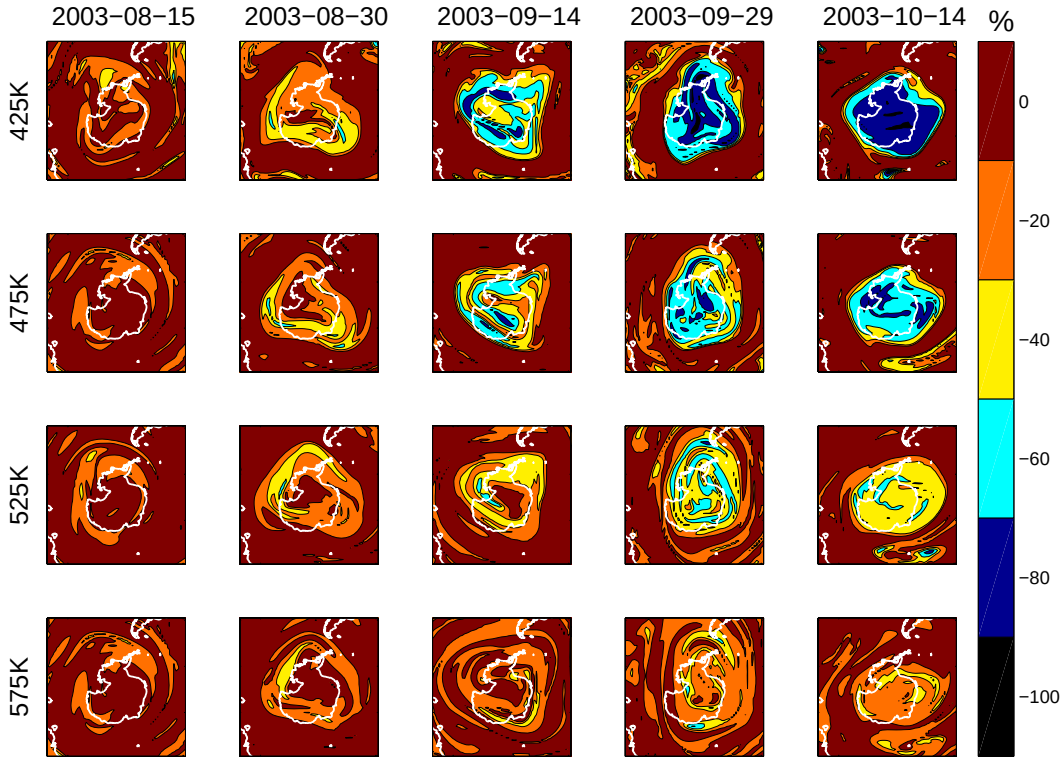

Fig. 7. Estimates of ozone depletion in the 2003 Antarctic spring made by comparing assimilated fields of Odin/SMR data to fields passively transported from 1 August.

ACPD
6, 9967–9994, 2006

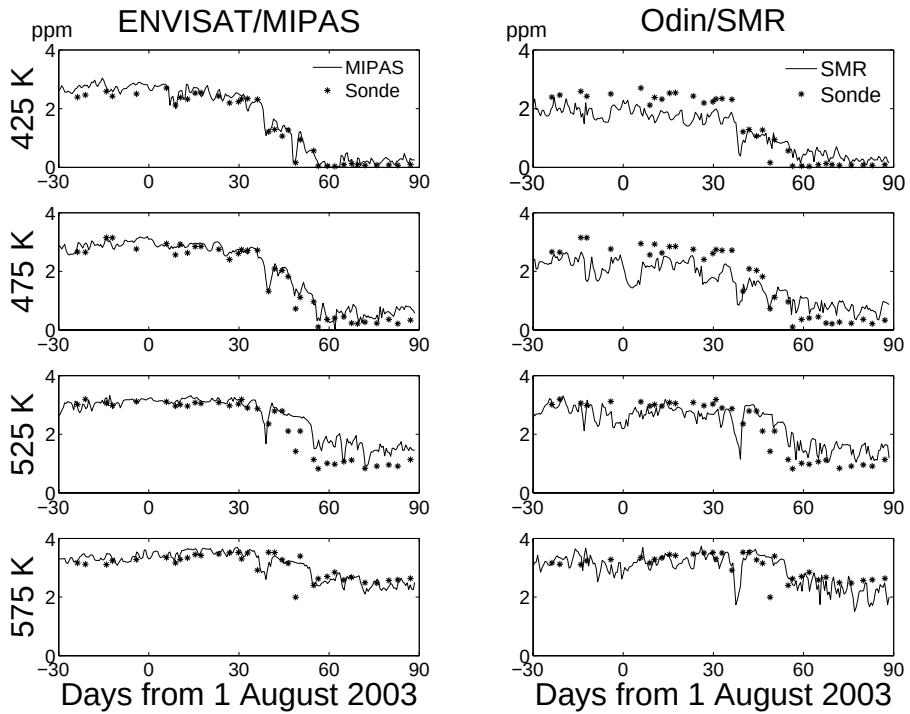

Fig. 8. Assimilated satellite data compared to balloon sonde measurements made over the south pole during the Antarctic winter of 2003. The solid lines represent the ozone mixing ratios found directly over the south pole in the DIAMOND model and the stars represent sonde measurements made at the same location. The sonde data has been obtained from the Network for the Detection of Stratospheric Change (NDSC) and is publicly available (see http://www.ndsc.ncep.noaa.gov).

ACPD
6, 9967–9994, 2006

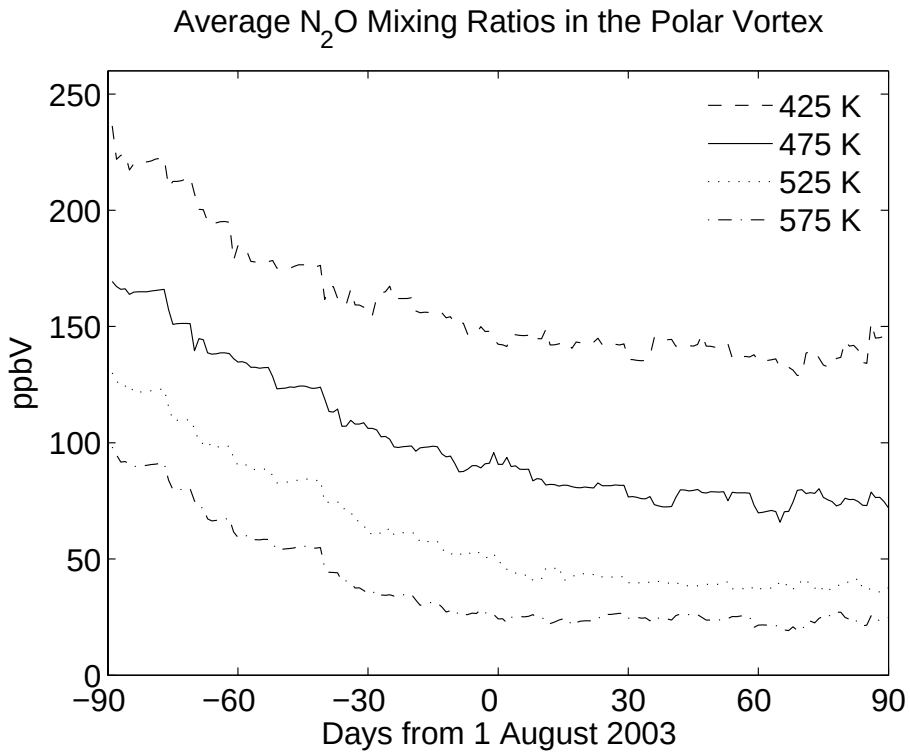

Fig. 9. Time evolution of the average N_2O mixing ratios on different potential temperature levels in the Antarctic polar vortex of 2003. The vortex averages have been obtained from assimilated fields of Odin/SMR N_2O data.

ACPD
6, 9967–9994, 2006

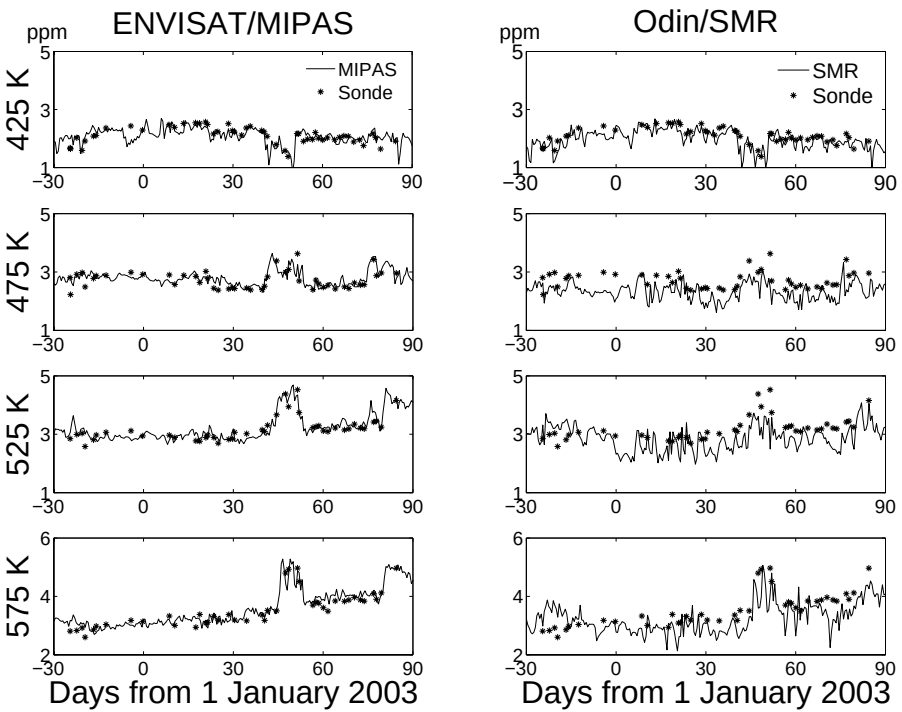

Fig. 10. Assimilated satellite data compared to balloon sonde measurements made over Ny-Ålesund (79° N, 12° E) during the Arctic winter of 2002/2003. Same source of data as in Fig. 8.

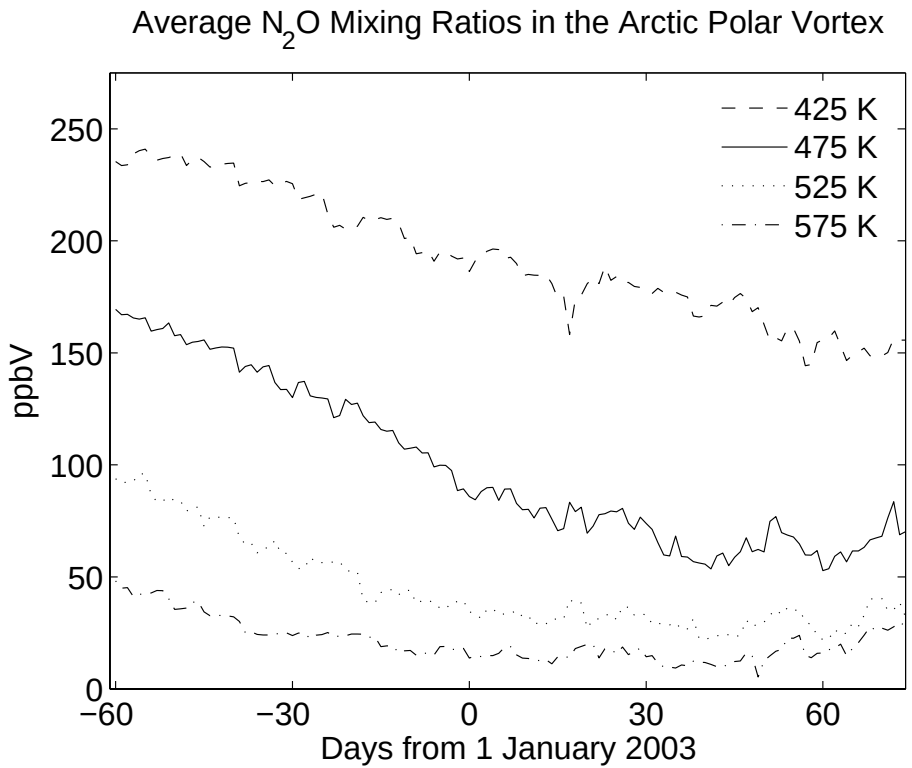

Fig. 11. Like Fig. 9 but the graphs describe average N_2O mixing ratios in the Arctic polar vortex of 2002/2003.

ACPD
6, 9967–9994, 2006

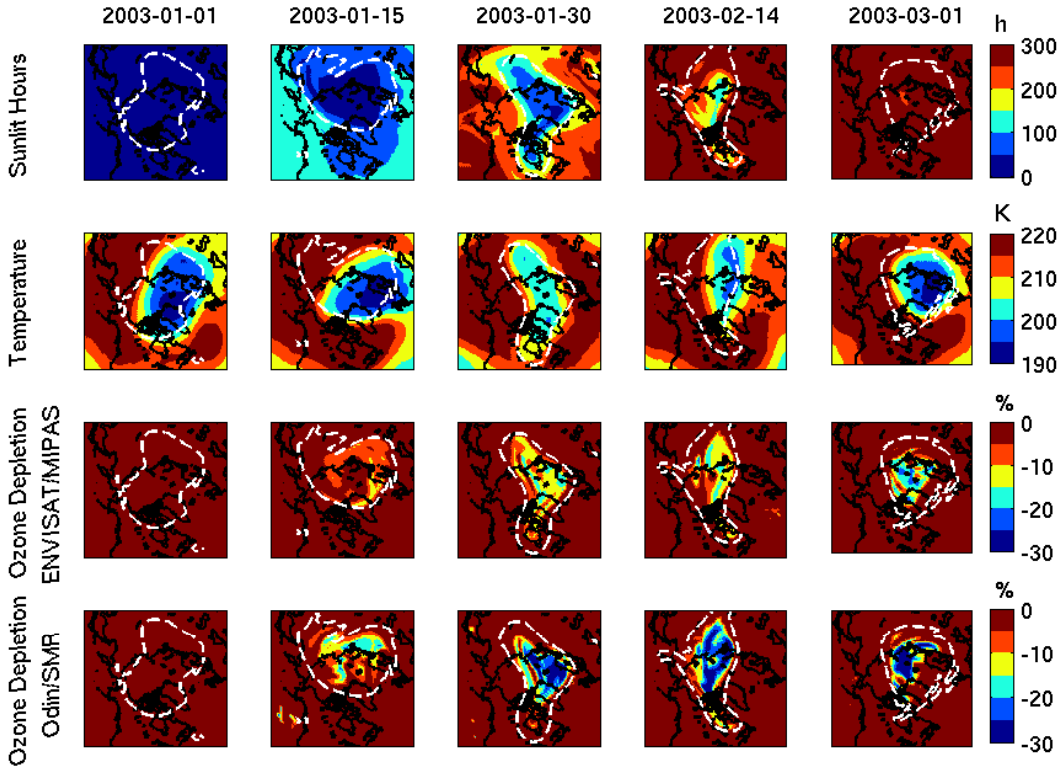

Fig. 12. A study of Arctic ozone depletion on the 475 K potential temperature level during the winter of 2002/2003 made by comparing assimilated fields of ENVISAT/MIPAS and Odin/SMR ozone data to fields passively transported from 1 January. The top fields represent the number of hours of sunlight that has fallen on the air masses in the model since 1 January and the dashed lines outline the border of the polar vortex.

ACPD
6, 9967–9994, 2006